Electrochimica Acta 403 (2022) 139632

Contents lists available at ScienceDirect

Electrochimica Acta

journal homepage: www.elsevier.com/locate/electacta

Study of oxygen-ion conductivity and luminescence in the ZrO_2 – Nd_2O_3 system: Impact of local heterogeneity

N.V. Lyskov[a,b], A.N. Shchegolikhin[c], D.N. Stolbov[d], I.V. Kolbanev[e], E. Gomes[f], J.C.C. Abrantes[f,g], A.V. Shlyakhtina[e,h,*]

[a] Institute of Problems of Chemical Physics RAS, Moscow Region, Chernogolovka, Russia
[b] HSE University, Myasnitskaya str. 20, 101000 Moscow, Russia
[c] Emanuel Institute of Biochemical Physics RAS, Moscow, Russia
[d] Department of Chemistry, Lomonosov Moscow State University, Leninskie Gory 1-3, Moscow, 119991, Russia
[e] N.N. Semenov Federal Research Center for Chemical Physics, Russian Academy of Sciences, Moscow, Russia
[f] proMetheus, Instituto Politécnico de Viana do Castelo, 4900-348 Viana do Castelo, Viana do Castelo, Portugal
[g] CICECO – Aveiro Institute of Materials, University of Aveiro, 3810-193 Aveiro, Portugal
[h] Kurnakov Institute of General and Inorganic Chemistry of the Russian Academy of Sciences, Moscow, Russia

ARTICLE INFO

Article history:
Received 21 September 2021
Revised 3 November 2021
Accepted 20 November 2021
Available online 28 November 2021

Keywords:
Zirconates
Pyrochlores
Fluorites
Oxygen-ion conductivity
Proton conductivity
Luminescence
Nanodomains

ABSTRACT

Stabilized fluorites and pyrochlores with different types of substitution in the (Nd_2O_3 – ZrO_2 system (NdZrO)) have been studied by Raman spectroscopy, X-ray diffraction, and impedance spectroscopy methods. Ionic and proton conductivity maps for 9 compositions in the NdZrO system are presented. Oxygen partial pressure measurements show a typical ionic conductor behavior, with a significantly increase of conductivity for $(Nd_{2-x}Zr_x)Zr_2O_{7+x/2}$ (x = 1.27) fluorite and $(Nd_{2-x}Zr_x)Zr_2O_{7+x/2}$ (x = 0.4, 0.2) pyrochlores. For the same compositions the strong luminescence was observed. Strong luminescence and high oxygen-ion conductivity of these solid solutions can be associated with the presence of phases with the different degree of structural disorder (tetragonal phase, fluorite) in local nanodomains in fluorite or pyrochlore matrix in the ZrO_2 – $Nd_2Zr_2O_7$ region. Really, Raman spectra of $(Nd_{2-x}Zr_x)Zr_2O_{7+x/2}$ (x = 0.5 – 0.2) solid solutions demonstrated the fluorite + pyrochlore structural type in the short-range order. Fluorite nanodomains in pyrochlore matrix (ZrO_2 – $Nd_2Zr_2O_7$ region) resulting from an order–disorder transition can only be detected at a radiation wavelength comparable to the fluorite nanodomain size. Thus, using Raman spectroscopy the broad isomorphism range in the ZrO_2 – $Nd_2Zr_2O_7$ system has been shown to be nonuniform.

1. Introduction

Fluorite and pyrochlore solid solutions in ZrO_2 – Ln_2O_3 systems have a wide range of properties suitable for a variety of practical applications: high oxygen ion conductivity, low thermal conductivity, high radiation resistance, luminescence [1–9]. As a rule, there is a relationship between the properties of compounds and solid solutions in these systems and a pronounced tendency toward the formation of cation and anion defects as a result of order–disorder transitions [10].

Yttria-stabilized zirconia (6 – 8% mol.% Y_2O_3) is currently used as an electrolyte material for fuel cells and thermal barrier coatings (TBCs) protecting the high-temperature details of aero-engine and gas turbine [11]. Lanthanide additives were studied as phosphors for noncontact thermometer detection of corrosion and defects in ZrO_2 – based TBCs [12,13]. However, the phase transition from the stabilized cubic phase to the tetragonal and monoclinic phases during service and the high sinterability of the fluorites above 1200 °C limit the use of ZrO_2 doped Y_2O_3 or Sc_2O_3 in its main applications. In view of this, pyrochlores are currently studied as an alternative to the stabilized fluorites and potential materials for the same purposes. Another application of the rare-earth zirconates is the development of more and more powerful semiconductor laser diodes operating at room temperature. There is an intensive search for materials for solid-state lasers that could be used as diodes for optical pumping. Previously, effort was concentrated on Nd- and Yb-doped single crystals and ceramics, but recently nanocrystalline $Nd_2Zr_2O_7$ has been shown to be a potential solid-state laser material for optical pumping of Nd^{3+} ions [14].

* Corresponding author: Kinetic and Catalysis, Institut Himiceskoj Fiziki Imeni N Semenova RAN, ul. Kosygina 4, Moscow 119991, Russia, 119991 Moscow, Russia.
E-mail address: annashl@inbox.ru (A.V. Shlyakhtina).

https://doi.org/10.1016/j.electacta.2021.139632
0013-4686/

Phase diagram data [15] show that, at low degrees of Nd substitution for Zr (6 –14 mol.% Nd_2O_3), there are stabilized cubic fluorite solid solutions. At higher degrees of substitution, there are a broad range of $(Nd_{2-x}Zr_x)Zr_2O_{7+x/2}$ ($14 \leq x < 33.3$ mol.% Nd_2O_3) pyrochlore solid solutions. Stoichiometric $Nd_2Zr_2O_7$ exists at 33.3 mol.% Nd_2O_3. A broad range of $Nd_2(Zr_{2-x}Nd_x)O_{7-x/2}$ solid solutions, in which partial Nd substitution for Zr is accompanied by oxygen vacancy formation, locates at (33.3 – 50 mol.% Nd_2O_3).

At room temperature, ZrO_2 has a monoclinic structure, which transforms into a tetragonal one above 1170 °C. The tetragonal-to-cubic phase transition is known to occur above 2370 °C [16,17]. Oxides (CaO or Ln_2O_3) can stabilize the high-temperature, cubic phase, with high oxygen ion conductivity, if the ionic radius of Ln^{3+} approaches that of Zr^{4+} and the oxide has a cubic structure [18]. According to more recent work, an important factor for the stabilization of the cubic phase at relatively low temperatures is the existence of a lower limit for its stabilization: the highest conductivity of $ZrO_2(Y_2O_3)$, the most widely used materials, was observed at 8 – 11 mol.% Y_2O_3, and that of $ZrO_2(Sc_2O_3)$, at 9 – 11 mol.% Sc_2O_3 [19]. It was assumed previously that the addition of higher dopant concentrations would reduce the ionic conductivity of the material as a result of the more active formation of associates of oxygen vacancies and dopant cations [20,21]. As shown in [20], the tendency toward the formation of associates is stronger in the case of a large difference between Zr^{4+} and Ln^{3+}. At the same time, according to Uehara et al. [22] and Arsent'ev et al. [23] the Ln_2O_3 – ZrO_2 systems with large and intermediate cations contain pyrochlore $Ln_2Zr_2O_7$ compounds that also have high oxygen ion conductivity, and the highest conductivity among the $Ln_2Zr_2O_7$ zirconates is offered by the europium and gadolinium compounds [2]. Comparatively recently, Shlyakhtina et al. [4] and Anithakumari et al. [5] studied $(Nd_{2-x}Zr_x)Zr_2O_{7+x/2}$ (18 – 33.3% Nd_2O_3) interstitial oxide ion conductors lying in the broad ZrO_2 – $Nd_2Zr_2O_7$ isomorphism range, with Nd substitution on the Zr site, some of which, in the range $x = 0.2$ to 0.4, had 700 °C oxygen ion conductivity as high as 5×10^{-3} to 1.78×10^{-2} S/cm, comparable to that of Li doped $Gd_2Zr_2O_7$ [24]. It should be emphasized that the broad isomorphism of the $Ln_2Zr_2O_7$ compounds in these systems is characteristic of the light and some intermediate lanthanide zirconates, whereas the Gd_2O_3 – ZrO_2 system, the most promising from the viewpoint of conductivity, has no broad $Gd_2Zr_2O_7$ isomorphism range [23].

Thus, in the case of the light and intermediate lanthanides, including the Ln_2O_3 – ZrO_2 (Ln = Nd – Gd) systems, a few maxima in conductivity are possible, whereas the R_2O_3 – ZrO_2 (R = Tb-Lu; Y, Sc) systems contain no pyrochlore compounds, and only ZrO_2-based fluorites (6–11 mol.% R_2O_3) demonstrate a maximum in conductivity. It seems likely that the maxima in the oxygen ion conductivity as a function of Ln_2O_3 content are due to the nonuniformity of the broad isomorphism range, which can include related and crystallographically similar pyrochlore and fluorite phases in different ratios. In particular, this conclusion is supported by the rather large R-factors obtained in Rietveld refinement of parameters of nonstoichiometric $(Nd_{2-x}Zr_x)Zr_2O_{7+x/2}$ ($x = 0.32$ – 0.48) pyrochlore solid solutions [4] and discrepancies between phase diagram data reported by different groups, e.g. for the Nd_2O_3–ZrO_2 system [15,25]. Unlike M. Perez Y Jorba [15], A. Rouanet assumes the presence of an $F + P$ two-phase field to the left of $Nd_2Zr_2O_7$ and a $P + F$ field to the right of it, thus denying the continuity of the fluorite–pyrochlore phase transition with increasing Nd_2O_3 content in the ZrO_2 – $Nd_2Zr_2O_7$ and $Nd_2Zr_2O_7$ – Nd_2O_3 regions at temperatures below 2000 °C [25]. To identify such phases, advanced structural spectroscopic methods are needed (XANES, Raman spectroscopy) [26].

In addition to the study of the oxygen ion conductivity of Ln_2O_3 – doped ZrO_2 and the $Ln_2Zr_2O_7$ -based pyrochlore zirconates, these compounds are of interest as luminescent materials owing to their chemical and photochemical stability, higher refractive index and lower phonon energies [27–31]. As pointed out in [30], the high-temperature, cubic phase of ZrO_2 can be stabilized not only by doping with Ln_2O_3 but also by reducing of the particle size to nanosize. $Nd_2Zr_2O_7$ nanoparticles synthesized by a molten salt synthesis method, were stabilized in the defect fluorite phase and showed an intense photoluminescence blue band and a weak green band after excited with 281 nm [31]. Thus, in the case of $Nd_2Zr_2O_7$ pyrochlores the cubic fluorite structure can be stabilized by reducing the crystallite size to the nanoscale, and it is nanomaterials that demonstrate luminescence. A previous research on the Er_2O_3-TiO_2 system revealed, for example, that $Er_2Ti_2O_7$ nanoparticles stabilized in defect fluorite-type structure ($T_{syn} \leq 700$ °C) exhibit a pink coloration. At higher temperature (800 °C), an atomic rearrangement into a pyrochlore structure significantly reduces this effect [32]. Because of this, the main direction in the research of LnZrO materials for luminescence is investigation of powders prepared, as a rule, by wet chemistry methods and consisting of nanoparticles (40–50 nm).

Light-emitting properties of pure and doped materials depend on the concentration of defects (e.g. oxygen vacancies), which are determined by the degree of crystallinity of the material and the dopant concentration and distribution. Thus, both the oxygen ion conductivity and luminescence properties of Ln_2O_3 doped ZrO_2 and the $Ln_2Zr_2O_7$ – based zirconates are related to their defect system, which depends significantly on their structure, composition, and crystallite size.

A number of similar systems [26,33–35] were reported to undergo nanostructuring, which was observed in rare-earth titanate solid solutions and was due to their structural inhomogeneity. As shown in a precision XANES spectroscopy study [26], the broad isomorphism range in the $Tm_2(Ti_{2-x}Tm_x)O_{7-x/2}$ (x = 0 – 0.67) system can be divided into three distinct regions: at x = 0 – 0.1, where only a pyrochlore phase exists; x = 0.134 – 0.563, where two pyrochlore phases coexist, one of which is thulium-deficient, and the other, thulium-enriched; and x = 0.563 – 0.67, where a defect fluorite phase prevails. The highest oxygen ion conductivity was found at x = 0.27, where the system was phase-separated into two pyrochlores.

Slow cooling (5 °C/h) of the $Ln_2(Ti_{2-x}Ln_x)O_{7-x/2}$ (Ln = Dy – Lu; $x = 0.67$) stuffed titanates with the fluorite structure made it possible to grow nanodomains of the pyrochlore phase to a micron size and detect them by X-ray diffraction [34,35]. Thus, pyrochlore nanodomains resulting from an order–disorder transition can only be detected at a radiation wavelength comparable to the domain size. It is, therefore, important to study such systems using not only diffraction methods but also spectroscopy.

In this paper, we report the ionic (oxygen ion and proton) conductivity (impedance spectroscopy) of compounds and solid solutions in the NdZrO system, starting from $(Nd_{2-x}Zr_x)Zr_2O_{7+x/2}$ (x = 1.27, 1.14, 0.96) stabilized fluorites and varying the composition to give $(Nd_{2-x}Zr_x)Zr_2O_{7+x/2}$ (x = 0.78, 0.67, 0.5, 0.4, 0.2, 0.1, 0.05) pyrochlore solid solutions, containing Zr substituted on the Nd site, and the stoichiometric compound $Nd_2Zr_2O_7$. In addition, we synthesized solid solutions containing Nd on the Zr site, $Nd_2(Zr_{2-x}Nd_x)O_{7-x/2}$ (x = 0.05, 0.1, 0.7), as potential oxygen vacancy and proton conductors. The objectives of this study were as follows: to compare the oxygen ion conductivity of the $(Nd_{2-x}Zr_x)Zr_2O_{7+x/2}$ (x = 1.27, 1.14, 0.96) solid solutions (Nd-stabilized fluorite structure), $(Nd_{2-x}Zr_x)Zr_2O_{7+x/2}$ (x = 0.78, 0.67, 0.5, 0.4, 0.2, 0.1, 0.05) solid solutions (containing excess Zr on the Nd site), undoped $Nd_2Zr_2O_7$, and $Nd_2(Zr_{2-x}Nd_x)O_{7-x/2}$ (x = 0.05, 0.1, 0.7) oxygen vacancy conductors; assess the proton conductivity of $Nd_2(Zr_{2-x}Nd_x)O_{7-x/2}$ (x = 0, 0.05, 0.1, 0.7); examine the effect of oxygen partial pressure on the total conductivity of the

Table 1
Samples under investigation.

Sample number	% Nd_2O_3	x in formula $(Nd_{2-x}Zr_x)Zr_2O_{7+x/2}$	x in formula $Nd_2(Zr_{2-x}Nd_x)O_{7-x/2}$	Structure according to Raman data	Structure according to XRD and ND data
1	10	1.27		T	F
2	12	1.14		$T + F$	F
3	15	0.96		F	F
4	18	0.78		F	P
5	20	0.67		F	P
6	23	0.5		$F + P$	P
7	23.5	0.48∼0.5		$F + P$	P
8	25	0.4		$F + P$	P
9	25.3	∼0.4		$F + P$	P
10	29	0.2		$F + P$	P
11	30.1	0.1		–	P
12	32.2	0.05		–	P
13	33.3	0		P	P
14	34.4		0.05	P	P
15	35.5		0.1	–	P
16	51		0.7	F	F

highest conductivity ceramics; evaluate the luminescence of the highest conductivity ceramics; and investigate the structure of $(Nd_{2-x}Zr_x)Zr_2O_{7+x/2}$ (x = 1.27, 1.14, 0.96,0.78, 0.67, 0.5, 0.4, 0.2, 0.1, 0.05) and $Nd_2(Zr_{2-x}Nd_x)O_{7-x/2}$ (x = 0, 0.05, 0.1, 0.67), by Raman spectroscopy.

2. Experimental

$(Nd_{2-x}Zr_x)Zr_2O_{7+x/2}$ pyrochlore materials ($0 \le x \le 1.27$) and $Nd_2(Zr_{2-x}Nd_x)O_{7-x/2}$ (x = 0.05, 0.1, 0.7) were prepared by mechanical activation of the oxide mixtures, sintered at high temperature (1550 °C, 10 h) of uniaxial pressed pellets. We used the following starting materials: Nd_2O_3 (99.9% purity, Ganzhou Wanfeng Advanced Materials Technology Co., Ltd.) and ZrO_2 (99%, Aldrich Chem Company, Inc.). The Nd_2O_3 was predried at 1000 °C for 2 h in air. Appropriate mixtures of the neodymium and zirconium oxides (∼21 g) were placed in an Aronov eccentric vibrating mill [36,37]. The oscillation amplitude and frequency of the vial containing balls and the powder were 0.5 cm and 50 Hz, respectively; the vial volume was 120 cm^3; and the ball-to-powder weight ratio was 15.

For clarity, Table 1 lists all of the ceramics prepared in this study and presents their compositions in two ways: (1) as a percentage of neodymium oxide (mol.% Nd_2O_3) and (2) as x in solid solutions with substitutions on the Nd site ($(Nd_{2-x}Zr_x)Zr_2O_{7+x/2}$ or Zr site $Nd_2(Zr_{2-x}Nd_x)O_{7-x/2}$).

Raman spectra of samples in the form of pellets and powders were taken without any sample preparation, on a Raman Station 400 dispersive Raman spectrometer (PerkinElmer, USA) at an optical resolution of 2 cm^{-1}. Excitation was provided by a 785-nm, 30-mW laser. The signal acquisition time was 30–60 s. X-ray diffraction (XRD) patterns of powder samples were collected at room temperature on a DRON-3 M automatic diffractometer (Cu K_α radiation, λ = 1.5418 Å, Bragg-reflection geometry, 35 kV, 28 mA) in the 2θ range 10° to 75° (scan step of 0.1° τ = 3 s.).

The microstructure of the ceramic samples was examined by scanning electron microscopy (SEM) on a JEOL JSM-6390LA, which was also used to perform X-ray fluorescence analysis and obtain selected-element X-ray maps. Using the SEM method, we analyzed the cation ratio on a freshly cleaved ceramic surface without polishing or thermal etching.

The electrical conductivity of all samples was characterized by two-probe AC impedance spectroscopy. Both faces of disk-shaped polycrystalline samples sintered as described above (2–3 mm thick with a diameter of 9–10 mm) were covered with Pt ink (ChemPur C3605) and fired at 950 °C for 30 min. Electrical conductivity measurements of the samples were performed on cooling using a P-5X potentiostat/galvanostat combined with frequency response analyzer module (Electrochemical Instruments, Ltd, Russia) over the frequency range of 500 kHz to 0.1 Hz at signal amplitude of 150 mV in the temperature range of 100–900 °C. Dry atmosphere was created by passing air through a KOH and wet atmosphere - through a water saturator held at 20 °C. The air flow rate was 130 mL/min. The measurements were made during cooling in wet and dry air, with isothermal holding at each temperature for 40 min.

Electrical characterization of some oxygen-ion conductors was carried out by impedance spectroscopy in the frequency range of 20 Hz to 1 MHz, with a signal amplitude of 200 mV(a moderately low value to avoid over-polarization and high enough to minimize signal interferences), using a Hewlett-Packard 4284A precision LCR bridge, as a function of temperature (300 - 1000 °C) and a function of the oxygen partial pressure, during reoxidation, after reduction with a mixture of 95% N_2 and 5% H_2, at 800, 850, 900, 950, and 1000 °C.

3. Results and discussion

3.1. Oxygen ion and proton conductivity in the Nd_2O_3 – ZrO_2 system

Fig. 1a show 3D mapping of total conductivity (dry air) in the Nd_2O_3 – ZrO_2 system. Fig. 1b presents oxygen ion and proton conductivity data in the composition range under discussion (10–51 mol.%) in the Nd_2O_3 – ZrO_2 system, which stands out among the Ln_2O_3 – ZrO_2 zirconate systems in that it has a broad isomorphism range symmetric with respect to $Nd_2Zr_2O_7$ according to phase diagram data [15]. It is worth noting first of all that the conductivity of the $(Nd_{2-x}Zr_x)Zr_2O_{7+x/2}$ (x = 0.4, 0.2) solid solutions, containing 25 – 29 mol.% Nd_2O_3 (Fig. 1, curves 6, 7), differs little from that of stabilized fluorite ZrO_2 (10 mol.% Nd_2O_3) ($(Nd_{2-x}Zr_x)Zr_2O_{7+x/2}$ (x = 1.27)) (Fig. 1, curve 9): ∼ 5 × 10^{-3} S/cm at 700 °C. The conductivity of the boundary composition ($(Nd_{2-x}Zr_x)Zr_2O_{7+x/2}$ (x = 0.96)), containing 15 mol.% Nd_2O_3, is a factor of 5 lower (Fig. 1, curve 8). The $(Nd_{2-x}Zr_x)Zr_2O_{7+x/2}$ (x = 0.05, 0.1) interstitial oxide ion conductors, rich in neodymium oxide, have a lower oxygen ion conductivity, ∼ 1 × 10^{-4} S/cm at 700 °C (Fig. 1, curves 4, 5), which however exceeds that of nominally stoichiometric pyrochlore $Nd_2Zr_2O_7$ (Fig. 1, curve 3).

Proton conductivity is observed in $Nd_2Zr_2O_7$ and the $Nd_2(Zr_{2-x}Nd_x)O_{7-x/2}$ (x = 0.05, 0.1) oxygen vacancy conducting solid solutions. As the degree of substitution increases, both the oxygen ion and proton contributions to their conductivity

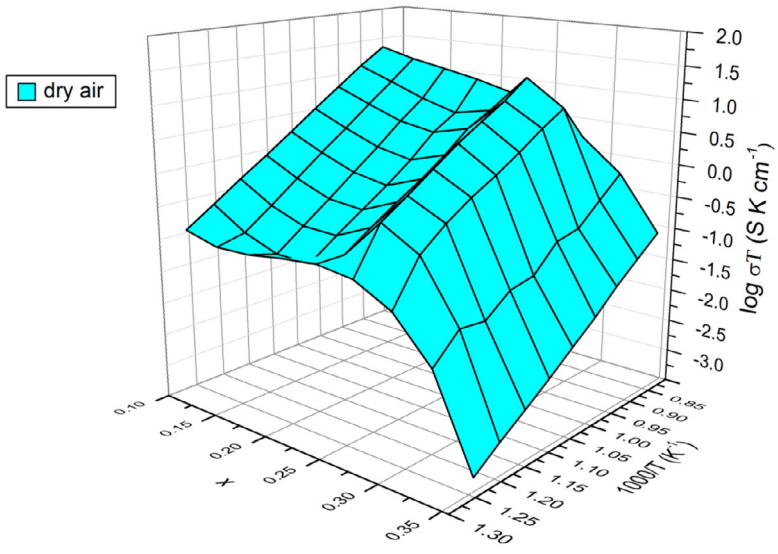

a

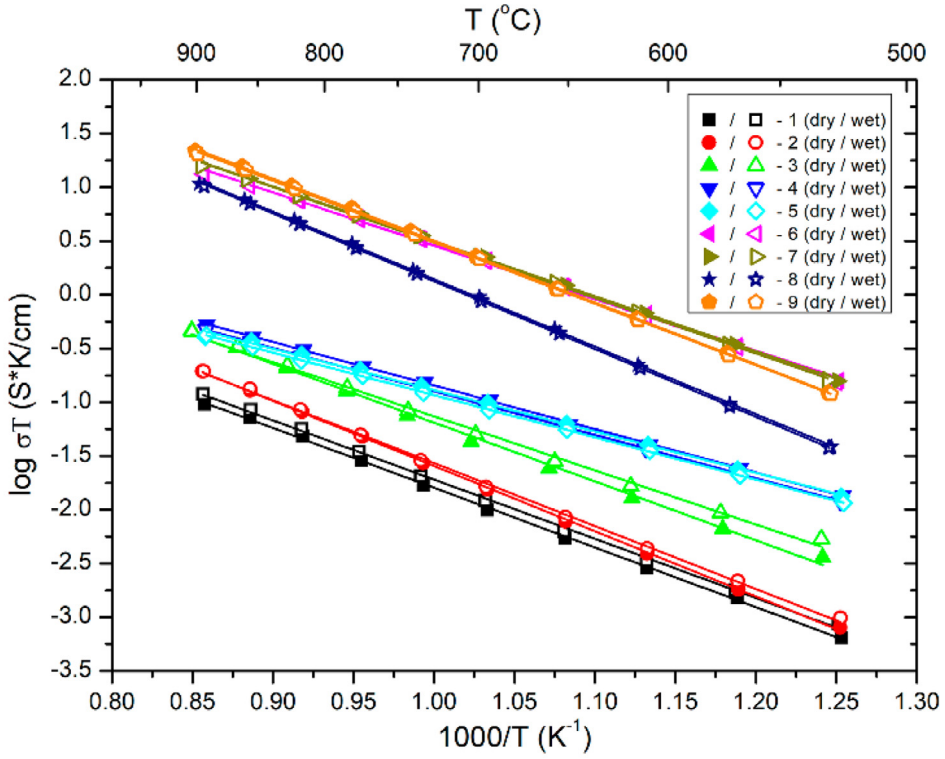

b

Fig. 1. (a) Total conductivity of the $Nd_2(Zr_{2-x}Nd_x)O_{7-x/2}$ and $(Nd_{2-x}Zr_x)Zr_2O_{7+x/2}$ solid solutions in dry air (3D image) and (b) total conductivity of the $Nd_2(Zr_{2-x}Nd_x)O_{7-x/2}$ and $(Nd_{2-x}Zr_x)Zr_2O_{7+x/2}$ solid solutions in dry and wet air (2D image):
1 - $Nd_2(Zr_{2-x}Nd_x)O_{7-x/2}$ ($x = 0.1$);
2 - $Nd_2(Zr_{2-x}Nd_x)O_{7-x/2}$ ($x = 0.05$);
3 - $Nd_2Zr_2O_7$;
4 - $(Nd_{2-x}Zr_x)Zr_2O_{7+x/2}$ ($x = 0.05$);
5 - $(Nd_{2-x}Zr_x)Zr_2O_{7+x/2}$ ($x = 0.1$);
6 - $(Nd_{2-x}Zr_x)Zr_2O_{7+x/2}$ ($x = 0.2$);
7 - $(Nd_{2-x}Zr_x)Zr_2O_{7+x/2}$ ($x = 0.4$);
8 - $(Nd_{2-x}Zr_x)Zr_2O_{7+x/2}$ ($x = 0.96$);
9 – $(Nd_{2-x}Zr_x)Zr_2O_{7+x/2}$ ($x = 1.27$).

Table 2
Data of SEM/EDX point analysis of some solid solution in the ZrO_2 - Nd_2O_3.

Sample number	% Nd_2O_3	x in formula $(Nd_{2-x}Zr_x)Zr_2O_{7+x/2}$	x in formula $Nd_2(Zr_{2-x}Nd_x)O_{7-x/2}$	Nd/Zroriginal ratio	Nd/Zr(SEM/EDX) data	Analysis area μm
1	10	1.27		0.22	0.26 ± 0.02	140 × 200
3	15	0.96		0.35	0.38 ± 0.02	
5	20	0.67		0.5	0.53 ± 0.02	
9	25.3	0.4		0.67	0.76 ± 0.02	
10	29	0.2		0.81	0.83 ± 0.10	
11	30.1	0.1		1	1.06 ± 0.02	
12	32.2	0.05		0.95	1.1 ± 0.03	
13	33.3	0		1	1.1 ± 0.02	
15	35.5		0.1	1.11	1.28 ± 0.02	

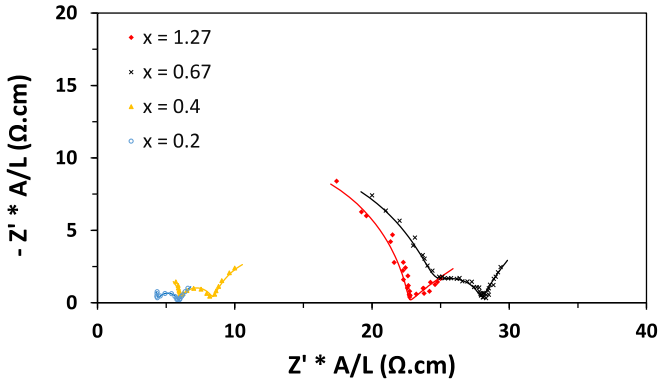

Fig. 2. 500 °C impedance spectra of the $(Nd_{2-x}Zr_x)Zr_2O_{7+x/2}$ (x = 1.27, 0.67, 0.4, 0.2) solid solutions.

decrease (Fig. 1, curves 1, 2). A similar effect for oxygen-ion conductivity, seemingly contradicting the defect chemistry, was observed previously in the titanate system Yb_2O_3 – TiO_2 [38]. It is reasonable to assume that the large Nd^{3+} cations can considerably narrow down oxygen diffusion channels, thereby reducing oxygen mobility in the system. Another possible cause is Nd_2O_3 volatility in the $Nd_2(Zr_{2-x}Nd_x)O_{7-x/2}$ oxygen vacancy conducting solid solutions and the associated deviations from the intended composition, as demonstrated below by EDX data (Table 2).

According to Fig. 1, the highest oxygen ion conductivity in the system was offered by the $(Nd_{2-x}Zr_x)Zr_2O_{7+x/2}$ (x = 0.4, 0.2) solid solutions and the $(Nd_{2-x}Zr_x)Zr_2O_{7+x/2}$ (x = 1.27) stabilized fluorite solid solution, which are the subject of the next sections.

3.2. Effect of oxygen partial pressure on the conductivity of the $(Nd_{2-x}Zr_x)Zr_2O_{7+x/2}$ (x = = 1.27, 0.96, 0.67, 0.4, 0.2, 0) solid solutions

Fig. 2 shows 500 °C impedance spectra of the $(Nd_{2-x}Zr_x)Zr_2O_{7+x/2}$ (x = 1.27, 0.67, 0.4, 0.2) solid solutions. Clearly, $(Nd_{2-x}Zr_x)Zr_2O_{7+x/2}$ (x = 0.2) has the lowest resistivity at this temperature, that of $(Nd_{2-x}Zr_x)Zr_2O_{7+x/2}$ (x = 0.4) pyrochlore is slightly higher, and the $(Nd_{2-x}Zr_x)Zr_2O_{7+x/2}$ (x = 1.27) stabilized fluorite solid solution, containing 10 mol.% Nd_2O_3, has still higher resistivity. Therefore, the pyrochlore solid solutions in which the Nd site is partially occupied by Zr ($(Nd_{2-x}Zr_x)Zr_2O_{7+x/2}$; x = 0.4, 0.2)) have the highest 500 °C conductivity.

Fig. 3 shows total conductivity as a function of oxygen partial pressure for the $(Nd_{2-x}Zr_x)Zr_2O_{7+x/2}$ (x = 1.27, 0.96, 0.67, 0.4, 0.2, 0) solid solutions at a higher temperature of 800 °C. At this temperature, the $(Nd_{2-x}Zr_x)Zr_2O_{7+x/2}$ (x = 0.2) solid solution has the highest conductivity, and the $(Nd_{2-x}Zr_x)Zr_2O_{7+x/2}$ (x = 0.96) solid solution, containing 15 mol.% Nd_2O_3 and located on the boundary between the tetragonal solid solutions and stabilized fluorites [4], has the second highest conductivity. The conductivity of $(Nd_{2-x}Zr_x)Zr_2O_{7+x/2}$ (x = 0.67, 0.4) is slightly lower. The conductivity of the stoichiometric ceramic $Nd_2Zr_2O_7$, ~ 1 × 10^{-4} S/cm at 800 °C, is 1.5 orders of magnitude lower than that of the highly conductive $(Nd_{2-x}Zr_x)Zr_2O_{7+x/2}$ (x = 0.2) material. Figs. 4a and b show total conductivity as a function of

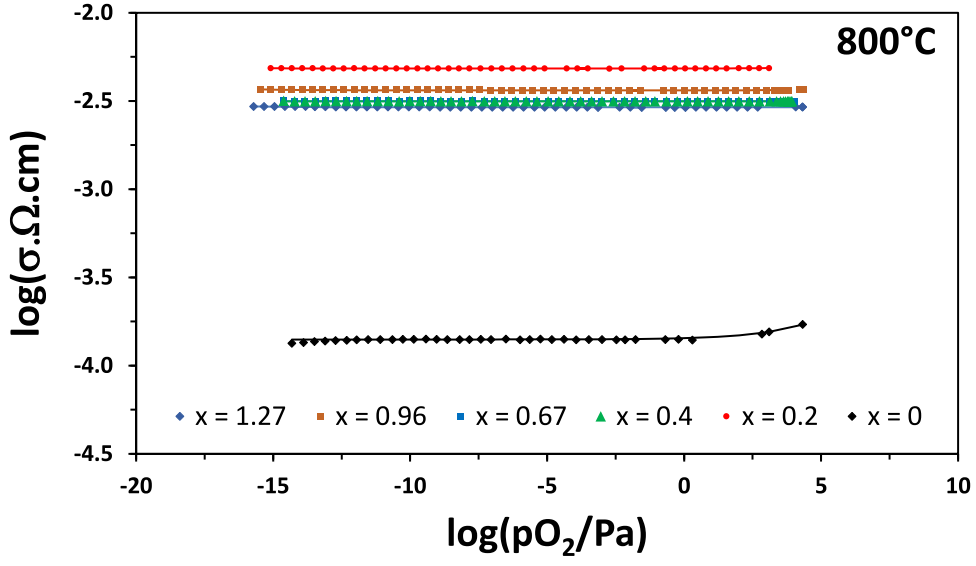

Fig. 3. Total conductivity as a function of oxygen partial pressure for the $(Nd_{2-x}Zr_x)Zr_2O_{7+x/2}$ (x = 1.27, 0.96, 0.67, 0.4, 0.2, 0) solid solutions.

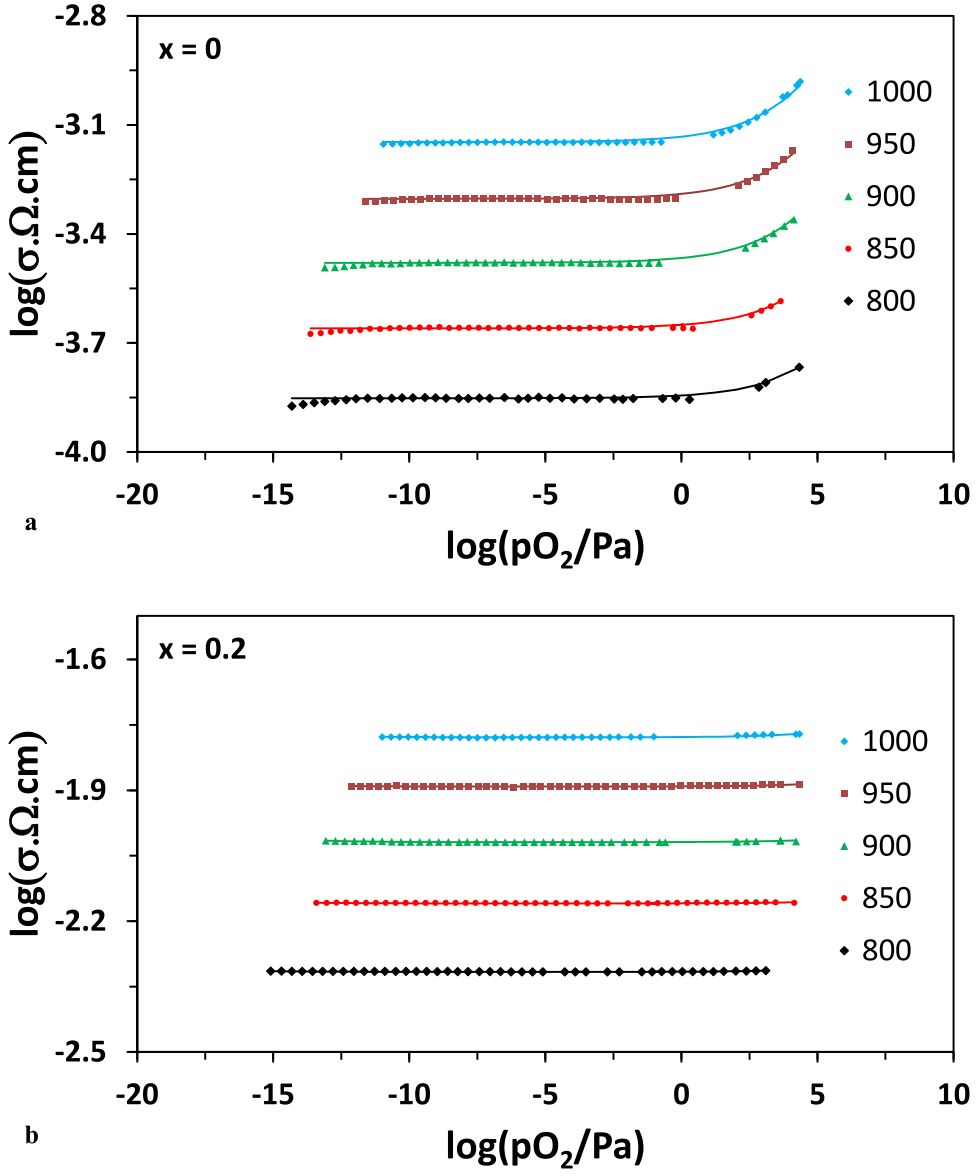

Fig. 4. Total conductivity as a function of oxygen partial pressure at different temperatures (a) for the nominally stoichiometric material $Nd_2Zr_2O_7$ and (b) the highest conductivity sample, $(Nd_{2-x}Zr_x)Zr_2O_{7+x/2}$ ($x = 0.2$).

oxygen partial pressure at different temperatures for the nominally stoichiometric material $Nd_2Zr_2O_7$ and the highest conductivity material, $(Nd_{2-x}Zr_x)Zr_2O_{7+x/2}$ ($x = 0.2$), respectively. It is seen that the region of pure oxygen ion conduction is shifted to higher oxygen partial pressures. Note also that the region of oxygen ion conduction decreases with increasing temperature and shifts to higher oxygen partial pressures in going from $(Nd_{2-x}Zr_x)Zr_2O_{7+x/2}$ ($x = 0.2$) to $Nd_2Zr_2O_7$.

3.3. Structure of the Nd_2O_3–ZrO_2 solid solutions studied by Raman spectroscopy

Almost all of the samples indicated in Table 1, except samples 11, 12, and 15, were characterized by Raman spectroscopy. The results are presented in Fig. 5. Analysis of the Raman spectra of the samples in the range 10 – 51 mol.% Nd_2O_3 shows that they can be divided into five groups according to the structure of their spectra. One group comprises the stabilized fluorites as shown by XRD [4]. According to their Raman spectra, samples 1 and 2 (Table 1), having the lowest (10 and 12 mol.% Nd_2O_3) content ($(Nd_{2-x}Zr_x)Zr_2O_{7+x/2}$ ($x = 1.27$, 1.14)) consist of a tetragonal phase [39] or a mixture of a tetragonal and a fluorite phase, rather than being pure fluorites. The next group has a fluorite-like short-range order and comprises samples 3–5 (Table 1), containing 15–20 mol.% Nd_2O_3 ($(Nd_{2-x}Zr_x)Zr_2O_{7+x/2}$ ($x = 0.96$, 0.78, 0.67). According to previous data [31], their spectra resemble that of $Nd_2Zr_2O_7$ nanoparticles prepared by molten salt synthesis, followed by low-temperature (650 °C) annealing. The three spectra have a broad band between 360 and 440 cm^{-1} due to F2g vibration of the disordered fluorite structure (Fig. 5, spectra 3–5). In addition, all three samples have a band in the range 540–630 cm^{-1}, which can be attributed to the F2g vibrational mode corresponding to the stretching of the Hf(Zr)–O bond. The line at ~500 cm^{-1} (A1g mode), which usually indicates the presence of a pyrochlore phase [40], is missing in spectra 3–5 in Fig. 5. Thus, we observe a fluorite-like short-range order in the $(Nd_{2-x}Zr_x)Zr_2O_{7+x/2}$ ($x = 0.96$, 0.78, 0.67) ceramics. Recall that, according to XRD and neutron diffraction data, the $(Nd_{2-x}Zr_x)Zr_2O_{7+x/2}$ ($x = 0.78$, 0.67) solid so-

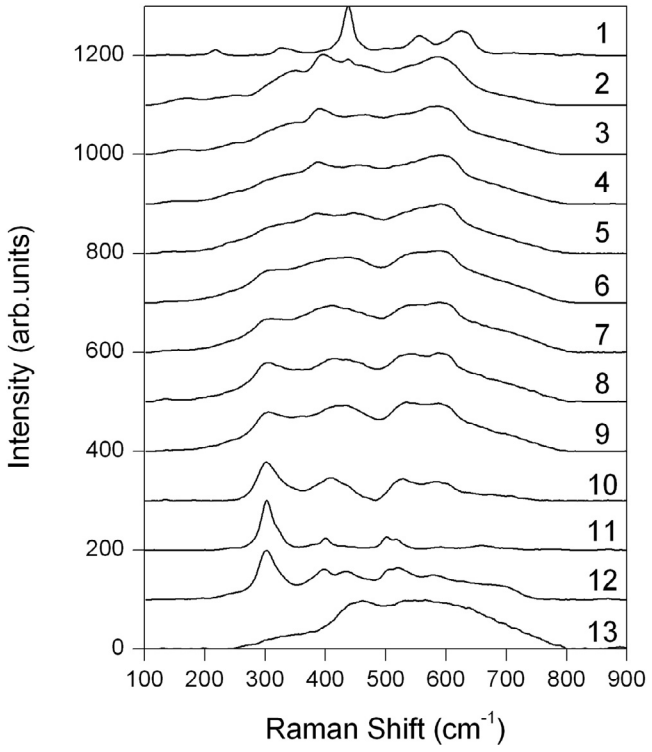

Fig. 5. Raman spectra:
(1) $(Nd_{2-x}Zr_x)Zr_2O_{7+x/2}$ (x = 1.27);
(2) $(Nd_{2-x}Zr_x)Zr_2O_{7+x/2}$ (x = 1.14);
(3) $(Nd_{2-x}Zr_x)Zr_2O_{7+x/2}$ (x = 0.96);
(4) $(Nd_{2-x}Zr_x)Zr_2O_{7+x/2}$ (x = 0.78);
(5) $(Nd_{2-x}Zr_x)Zr_2O_{7+x/2}$ (x = 0.67);
(6) $(Nd_{2-x}Zr_x)Zr_2O_{7+x/2}$ (x = 0.5);
(7) $(Nd_{2-x}Zr_x)Zr_2O_{7+x/2}$ (x = 0.5);
(8) $(Nd_{2-x}Zr_x)Zr_2O_{7+x/2}$ (x = 0.4);
(9) $(Nd_{2-x}Zr_x)Zr_2O_{7+x/2}$ (x = 0.4);
(10) $(Nd_{2-x}Zr_x)Zr_2O_{7+x/2}$ (x = 0.2);
(11) $Nd_2Zr_2O_7$;
(12) $Nd_2(Zr_{2-x}Nd_x)O_{7-x/2}$ (x = 0.05);
(13) $Nd_2(Zr_{2-x}Nd_x)O_{7-x/2}$ (x = 0.7).

lutions have the pyrochlore structure [4]. A similar discrepancy between diffraction and spectroscopy data was reported by Mullens et al. [26] for stuffed pyrochlores TmTiO system.

The third group comprises the solid solutions containing 23–29 mol.% Nd_2O_3 $(Nd_{2-x}Zr_x)Zr_2O_{7+x/2}$ (x = 0.5, 0.4, 0.2)). According to the Raman spectroscopy data (Fig. 5, spectra 6 – 10), they consist of a mixture of a nanoparticulate fluorite phase (with the main bands at 360 – 440 and 540 – 630 cm^{-1} present) and a pyrochlore phase (the main lines at ~300, 403, 520, and 590 cm^{-1}). Note that, in the spectrum of the highest conductivity sample, $(Nd_{2-x}Zr_x)Zr_2O_{7+x/2}$ (x = 0.2), the 500 cm^{-1} line (A1g mode), the signature of the ordered pyrochlore structure [39,40], is missing.

According to XRD and neutron diffraction data, the $(Nd_{2-x}Zr_x)Zr_2O_{7+x/2}$ (x = 0.5, 0.4, 0.2) solid solutions have a pyrochlore-like long-range order and the corresponding superstructure reflections (111), (311), (331), (511) were presented in the XRD and ND [4], whereas according to the present Raman spectroscopy data they consist of a mixture of a nanoparticulate fluorite phase and a pyrochlore phase.

The spectra of nominally stoichiometric pyrochlore $Nd_2Zr_2O_7$ and the $Nd_2(Zr_{2-x}Nd_x)O_{7-x/2}$ (x = 0.1) oxygen vacancy conducting solid solution based on it are typical of pyrochlores and contain the 500 cm^{-1} line (A1g mode), but, since Nd doping on the Zr site produces oxygen vacancies, thus increasing the defect density in the system, this line in the spectrum of the $Nd_2(Zr_{2-x}Nd_x)O_{7-x/2}$

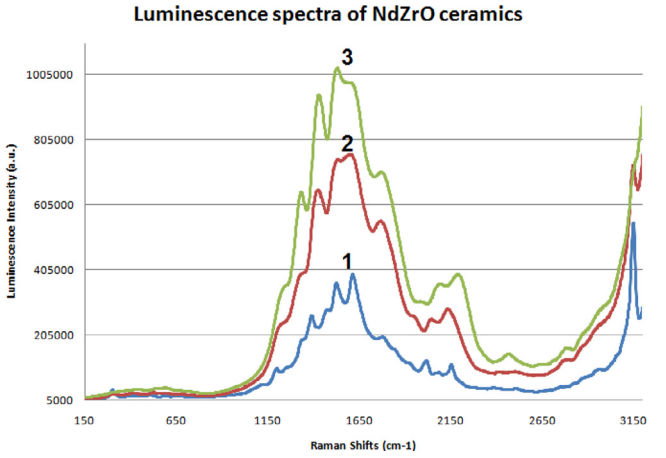

Fig. 6. Luminescence spectra of the (1) $Nd_2Zr_2O_7$, (2) $(Nd_{2-x}Zr_x)Zr_2O_{7+x/2}$ (x = 0.2), and (3) $(Nd_{2-x}Zr_x)Zr_2O_{7+x/2}$ (x = 0.5).

(x = 0.1) solid solution is broader than that in the spectrum of stoichiometric neodymium zirconate (Fig. 5, spectra 11, 12). A1g vibration mode gives important information of the force constant provided by the oscillations of La–O and Hf–O in lanthanum hafnate [39]. The diffraction and spectroscopy data for $Nd_2Zr_2O_7$ and $Nd_2(Zr_{2-x}Nd_x)O_{7-x/2}$ (x = 0.05, 0.1) agree well: in both cases, the pyrochlore structure is observed. Finally, the spectrum of the $Nd_2(Zr_{2-x}Nd_x)O_{7-x/2}$ (x = 0.7) fluorite phase, containing 51 mol.% Nd_2O_3 (Fig. 5, spectrum 13) and consisting of micron grains, is typical of fluorite phases and is dominated by a broad vibrational peak due to the uniform oxygen distribution over all eight positions, which leads to significant structural disorder [31]. In this case too, the diffraction data are well consistent with the spectroscopy results.

3.4. Broadband luminescence of the $(Nd_{2-x}Zr_x)Zr_2O_{7+x/2}$ (x = 0.5; 0.2) highly conductive solid solutions in comparison with stoichiometric $Nd_2Zr_2O_7$

Fig. 6 shows luminescence spectra of the $(Nd_{2-x}Zr_x)Zr_2O_{7+x/2}$ (x = 0.2) solid solution, having the highest conductivity, and the $(Nd_{2-x}Zr_x)Zr_2O_{7+x/2}$ (x = 0.5) solid solution. According to the data in Fig. 5, they have similar Raman spectra. Also shown for comparison in Fig. 6 is the spectrum of stoichiometric $Nd_2Zr_2O_7$. All three samples have similar spectra, with bright luminescence in the range 1150 – 2350 cm^{-1}. Note that the broadband luminescence intensity rises in the order: $Nd_2Zr_2O_7$ < $(Nd_{2-x}Zr_x)Zr_2O_{7+x/2}$ (x = 0.2) < $(Nd_{2-x}Zr_x)Zr_2O_{7+x/2}$ (x = 0.5).

Borik et al. [41] reported luminescence of partially Y-stabilized and Nd^{3+}doped ZrO_2, grown by induction skull melting. They assumed that the luminescence was due to Nd^{3+} localization in one of two tetragonal phases differing in parameters in single crystals with a well-developed nanodomain structure. In their study, nanoobjects (nanodomains) were formed at high temperatures as a result of the high-temperature tetragonal-to-fluorite phase transition, unlike nanopowders prepared by various methods at relatively low temperatures [31]. Fig. 7. shows the total spectrum (Raman and luminescence components) of $(Nd_{2-x}Zr_x)Zr_2O_{7+x/2}$ (x = 1.27), which is similar in shape to that reported by Borik et al. [41]. In our study the strong luminescence of $(Nd_{2-x}Zr_x)Zr_2O_{7+x/2}$ (x = 1.27) ceramic may be due to Nd^{3+} localization in the tetragonal phase nanodomains in accordance with Raman spectra (Fig. 5, scan 1).

Thus, the present results demonstrate that the fluorite phase in the ZrO_2 – $Nd_2Zr_2O_7$ system is stabilized at a higher rare-earth ox-

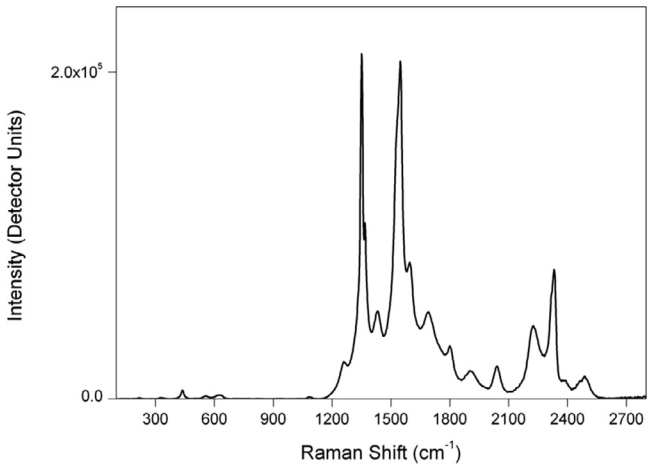

Fig. 7. Total spectrum of $Nd_2(Zr_{2-x}Nd_x)O_{7+x/2}$ (x = 1.27) (Raman + Luminescence parts).

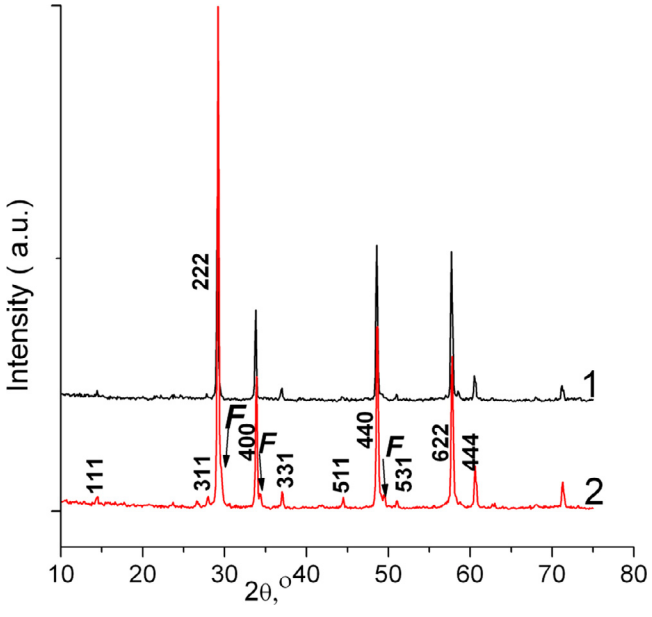

Fig. 8. XRD data for the $Nd_2(Zr_{2-x}Nd_x)O_{7+x/2}$ (x = 0.2) solid solution: (a) as-prepared, (2) after cooling at 0.3 °C/h from 1550 to 1300 °C.

ide concentration than in the ZrO_2 – R_2O_3 (R = = Y, Sc) systems and that fluorite-like short-range order is stable in the range 12 < Nd_2O_3% < 20. However, the presence of the tetragonal phase nanodomains should be noted for composition with 12 mol.% Nd_2O_3 (Fig. 5, scan 2).

3.5. Growth of nanodomains in the $(Nd_{2-x}Zr_x)Zr_2O_{7+x/2}$ (x = = 0.2) highly conductive solid solution

The $(Nd_{2-x}Zr_x)Zr_2O_{7+x/2}$ (x = 0.2) highly conductive ceramic was reheated to 1550 °C, slowly cooled at 3 °C/h to 1300 °C, and then furnace-cooled. Fig. 8 presents XRD data for the as-prepared and slowly cooled $(Nd_{2-x}Zr_x)Zr_2O_{7+x/2}$ (x = 0.2) ceramic. It is seen that, after such cooling, there is an additional phase, which can be identified, according to ICDD PDF data, as the fluorite phase $Nd_{0.2}Zr_{0.8}O_{1.9}$ (ICDD PDF 78–1301) or $Nd_{0.25}Zr_{0.75}O_{1.875}$ (ICDD PDF 28–678).

Thus, we were able to grow fluorite structure nanodomains large enough to be detected by not only spectroscopy but also XRD. Clearly, the two-phase system containing nanodomains of the fluorite phase together with the pyrochlore phase in the composition range near $Nd_2Zr_2O_7$ is unstable, so reducing the cooling rate allows nanodomain growth to be initiated.

3.6. Microstructure of the ZrO_2 – Nd_2O_3 solid solutions

The microstructure of some of the solid solutions was examined by SEM. The results are presented in Fig. 9 and Table 2. Note that the composition of most sample differed little from the intended one, except for the $(Nd_{2-x}Zr_x)Zr_2O_{7+x/2}$ (x = 0.4) and $Nd_2(Zr_{2-x}Nd_x)O_{7-x/2}$ (x = 0.1) samples. The tetragonal and stabilized fluorite phases in $(Nd_{2-x}Zr_x)Zr_2O_{7+x/2}$ (x = 1.27, 0.96, 0.67) typically consisted of large grains ~10 μm in size (Figs. 9a, b, and c). $(Nd_{2-x}Zr_x)Zr_2O_{7+x/2}$ (x = 1.27) had an unusual morphology (Fig. 9a). According to Raman spectroscopy data, this material consisted of a tetragonal phase, was a good conductor, and had bright luminescence. Clearly, this ceramic consisted of nanograins, some of which formed large intergrowths, up to 10 μm in size, and some were located at grain boundaries. The $(Nd_{2-x}Zr_x)Zr_2O_{7+x/2}$ (x = 0.67) ceramic had a smaller grain size.

The $(Nd_{2-x}Zr_x)Zr_2O_{7+x/2}$ (x = 0.4, 0.2) highly conductive ceramics differed insignificantly in grains size from $(Nd_{2-x}Zr_x)Zr_2O_{7+x/2}$ (x = 0.1), which had a factor of 5 lower conductivity. Characteristically, it ranged widely in grain size, from 3 to 10 μm. Further increasing the Nd content of $(Nd_{2-x}Zr_x)Zr_2O_{7+x/2}$ (x = 0.05) reduced

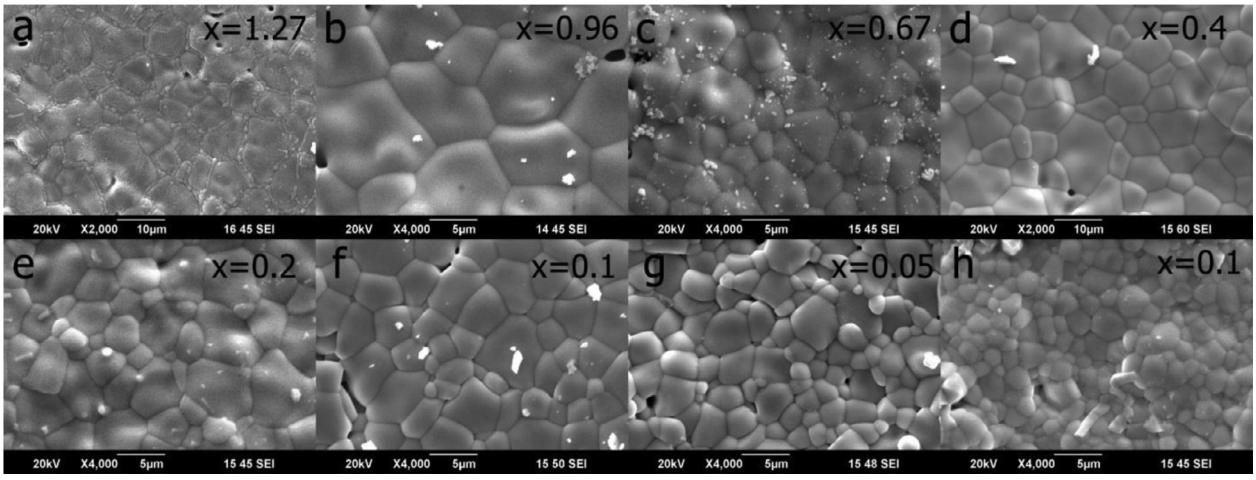

Fig. 9. Microstructure of some solid solutions: (a) $(Nd_{2-x}Zr_x)Zr_2O_{7+x/2}$ (x = 1.27), (b) $(Nd_{2-x}Zr_x)Zr_2O_{7+x/2}$ (x = 0.96), (c) $(Nd_{2-x}Zr_x)Zr_2O_{7+x/2}$ (x = 0.67), (d) $(Nd_{2-x}Zr_x)Zr_2O_{7+x/2}$ (x = 0.4), (e) $(Nd_{2-x}Zr_x)Zr_2O_{7+x/2}$ (x = 0.2), (f) $(Nd_{2-x}Zr_x)Zr_2O_{7+x/2}$ (x = 0.1);(g) $Nd_2(Zr_{2-x}Nd_x)O_{7-x/2}$ (x = 0.05), (h) $Nd_2(Zr_{2-x}Nd_x)O_{7-x/2}$ (x = 0.1).

the grain size, which was limited to 5 μm. This sample was more uniform, with a very small scatter in grain size. According to SEM data, the $Nd_2(Zr_{2-x}Nd_x)O_{7-x/2}$ ($x = 0.1$) oxygen vacancy conductor, with low conductivity, had the smallest average grain size: ~2 μm.

4. Conclusions

The broad isomorphism range in the ZrO_2 – Nd_2O_3 system has been investigated by impedance and Raman spectroscopy techniques. In the ZrO_2 – $Nd_2Zr_2O_7$ subsystem, we have studied $(Nd_{2-x}Zr_x)Zr_2O_{7+x/2}$ ($x = 1.27$, 1.14, 0.96) solid solutions with a stabilized fluorite structure and $(Nd_{2-x}Zr_x)Zr_2O_{7+x/2}$ ($x = 0.78$, 0.67, 0.5, 0.4, 0.2, 0.1, 0.05) substitutional solid solutions with the pyrochlore structure in accordance with preliminary XRD and neutron diffraction study [4]. In the $Nd_2Zr_2O_7$ – Nd_2O_3 subsystem, we have studied $Nd_2(Zr_{2-x}Nd_x)O_{7-x/2}$ ($x = 0$, 0.05, 0.1, 0.7) substitutional solid solutions. A narrow range of proton conduction has been found in $Nd_2(Zr_{2-x}Nd_x)O_{7-x/2}$ ($x = 0$, 0.05, 0.1). The $(Nd_{2-x}Zr_x)Zr_2O_{7+x/2}$ ($x = 0.5$, 0.4, 0.2) solid solutions, consisting of a mixture of a nanostructured fluorite phase and a pyrochlore phase, rather than being homogeneous, have high oxygen ion conductivity and appreciable broadband luminescence. All the properties, including high conductivity and luminescence, that differentiate the $(Nd_{2-x}Zr_x)Zr_2O_{7+x/2}$ ($x = 0.5$, 0.4, 0.2) solid solutions from the other materials studied in the ZrO_2 – Nd_2O_3 system are obviously due to the presence of fluorite structure nanodomains in a pyrochlore structure matrix. Fluorite nanodomains in a pyrochlore matrix are difficult to detect by diffraction techniques (XRD, synchrotron XRD, or neutron diffraction), but this can be done by spectroscopic methods (Raman scattering or XANES) or by growing nanodomains from such inhomogeneous solid solutions using cooling rates as low as 3 °C/h in the 1550–1300 °C temperature range. High conductivity and strong luminescence have also been found in the stabilized fluorite phase $(Nd_{2-x}Zr_x)Zr_2O_{7+x/2}$ ($x = 1.27$), in long-range order, which consists of a tetragonal phase nanodomains according to Raman spectroscopy data and has an unusual morphology.

Declaration of Competing Interest

The authors declare that they have no known competing financial interests or personal relationships that could have appeared to influence the work reported in this paper.

Credit authorship contribution statement

N.V. Lyskov: Investigation, Formal analysis. **A.N. Shchegolikhin:** Investigation, Data curation. **D.N. Stolbov:** Investigation, Formal analysis. **I.V. Kolbanev:** Resources. **E. Gomes:** Investigation. **J.C.C. Abrantes:** Investigation, Methodology. **A.V. Shlyakhtina:** Methodology, Writing – review & editing.

Acknowledgement

The support of this work by the Russian Science Foundation (Project 18-13-00025 - XRD, luminescence, Raman spectroscopy data) is gratefully acknowledged. Conductivity measurements of the samples in dry and wet air were supported in accordance with the state task for IPCP RAS, state registration No. АААА-А19-119061890019-5 and into frameworks of the state task for FRCCP "Nanostructured systems of a new generation with unique functional properties".

Supplementary materials

Supplementary material associated with this article can be found, in the online version, at doi:10.1016/j.electacta.2021.139632.

References

[1] T. Shimura, M. Komori, H. Iwahara, Ionic conduction in pyrochlore – type oxides containing rare-earth elements at high temperature, Solid State Ion. 86-88 (1996) 685–689.
[2] H. Yamamura, H. Nishino, K. Kakinuma, K. Nomura, Electrical conductivity anomaly around fluorite-pyrochlore phase boundary, Solid State Ion. 158 (2003) 359–365.
[3] A.V. Shlyakhtina, J.C.C. Abrantes, E. Gomes, A.N. Shchegolikhin, G.A. Vorobieva, K.I. Maslakov, L.G. Shcherbakova, Effect of Pr^{3+}/Pr^{4+} ratio on the oxygen ion transport and thermomechanical properties of the pyrochlore and fluorite phases in the ZrO_2–Pr_2O_3 system, Int. J. Hydr. Energy 41 (2016) 9982–9992.
[4] A.V. Shlyakhtina, D.A. Belov, A.V. Knotko, M. Avdeev, I.V. Kolbanev, G.A. Vorobieva, O.K. Karyagina, L.G. Shcherbakova, Oxide ion transport in $(Nd_{2-x}Zr_x)Zr_2O_{7+\delta}$ electrolytes by an interstitial mechanism, J. Alloys Compd. 603 (2014) 274–281.
[5] P. Anithakumari, V. Grover, C. Nandi, K. Bhattacharyya, A.K. T.yagi, Utilizing non-stoichiometry in $Nd_2Zr_2O_7$ pyrochlore: exploring superior ionic conductors, RSC Adv. 6 (2016) 97566–97579.
[6] Y. Zhang, M. Xie, F. Zhou, X. Cui, X. Lei, X. Song, S. An, Low thermal conductivity in $La_2Zr_2O_7$ pyrochlore with A-site partially substituted with equimolar Yb_2O_3 and Er_2O_3, Ceram. Int. 40 (2014) 9151–9157.
[7] X. Lu, X. Shu, D. Shao, S. Chen, H. Zhang, X. Yuan, F. Chi, Radiation stability of $Gd_2Zr_2O_7$ and $Nd_2Ce_2O_7$ ceramics as nuclear waste forms, Ceram. Int. 44 (2018) 760–765.
[8] G.M. Mustafa, S. Atiq, S.K. Abbas, S. Riaz, S. Naseem, Tunable structural and electrical impedance properties of pyrochlores based Nd doped lanthanum zirconate nanoparticles for capacitive applications, Ceram. Int. 44 (2018) 2170–2177.
[9] H. Chander, Development of nanophosphors - A review, Mater. Sci. Eng. R. 49 (2005) 113–155.
[10] J. Shamblin, C.L. Tracy, R.I. Palomares, E.C. O'Quinn, R.C. Ewing, J. Neuefeind, M. Feygenson, J. Behrens, C. Trautmann, M. Lang, Similar local order in disordered fluorite and aperiodic pyrochlore structures, Acta Mater. 144 (2018) 60–67.
[11] X. Wei, G. Hou, Y. An, P. Yang, X. Zhou, H. Zhou, J. Chen, Effect of doping CeO_2 and Sc_2O_3 on structure, thermal properties and sintering resistance of YSZ, Ceram. Int. 47 (5) (2021) 6875–6883.
[12] E. Eldridge, Erosion-indicating thermal barrier coatings using luminescent sublayers, J. Am. Ceram. Soc. 89 (10) (2006) 3252–3254, doi:10.1111/j.1551-2916.2006.01210.x.
[13] M.M. Gentleman, D.R. Clarke, Luminescence sensing of temperature in pyrochlore zirconate materials for thermal-barrier coatings, Surf. Coat. Technol. 200 (2005) 1264–1269.
[14] T. Feng, D.R. K.lark, D. Jiang, J. Xia, J. Shi, Neodymium zirconate ($Nd_2Zr_2O_7$) transparent ceramics as a solid state laser material, Appl. Phys. Lett. 98 (2011) 151105, doi:10.1063/1.3579526.
[15] M. Perez, Y. Jorba, ZrO_2-rare-earth oxides systems, Ann. Chim. 7 (1962) 479–511.
[16] D.K. Smith, C.F. Cline, Verification of existence of cubic zirconia at high temperature, J. Amer. Ceram. Soc. 45 (1962) 249–250.
[17] N. Claussen, M. Ruhle, A. Heuer (Eds.), Phase Transformations in ZrO_2-containing ceramics: II, the Martensitis Reaction in t-ZrO_2, Science and Technology of Zirconia II, 1983.
[18] O. Ruff, F. Ebert, Refractory ceramics: I. The forms of zirconium dioxide, Z. Anorg. Allg. Chem. 180 (1929) 19–41.
[19] S.P.S. Badwal, F.T. Ciacchi, S. Rajendran, J. Drennan, An investigation of conductivity, microstructure and stability of electolyte compositions in the system 9 mol% $(Sc_2O_3$-$Y_2O_3)$-$ZrO_2(Al_2O_3)$, Solid State Ion. 109 (1998) 167–186.
[20] V.V. Kharton, F.M.B. Marques, A. Atkinson, Transport properties of solid oxide electrolyte ceramics: a brief review, Solid State Ion. 174 (2004) 135–149.
[21] F. Yang, Electrical and thermal properties of yttria-stabilized zirconiz (YSZ) - based ceramic materials, PhD Materials Science Centre, School of Materials, University of Manchester, 2011.
[22] T. Uehara, K. Koto, F. Kanamaru, Stability and antiphase domain structure of the pyrochlore solid solution in the ZrO_2-Gd_2O_3 system, Solid State Ion. 23 (1987) 137–143.
[23] P.A. Arsent'ev, V.B. Glushkova, A.A. Evdokimov, E.K. Keler, V.B. Kravchenko, M.V. Kravchinskaya, V.A. Krzhizhanovskaya, A.K. Kuznetsov, Kh.M. Kurbanov, A.V. Potemkin, P.A. Tikhonov, M.N. Tseitlin, Rare-earth compounds: Zirconates, Hafnates, Niobates, Tantalates, and Antimonates, Nauka, Moscow, 1985.
[24] I.A. Anokhina, I.E. Animitsa, V.I. Voronin, V.B. Vykhodets, T.E. Kurennykh, N.G. Molchanova, A.I. Vylkov, A.E. Dedyukhin, Y.P. Zaikov, The structure and electrical properties of lithium doped pyrochlore Gd2Zr2O7, Ceram. Intern. 47 (2) (2021) 1949–1961.
[25] A. Rouanet, Contribution a l·etude des systemes zirconia – oxides des lanthanides au voisinage de la fusion: memoire de these, Rev. Intern. Hautes Temt. et Refract. 8 (1971) 161–180.
[26] B.G. Mullens, Z. Zhang, M. Avdeev, H.E.A. Brand, B.C.C. Cowie, M.S. Muzquiz, B.J. K.ennedy, Effect of long and short-range disorder on the oxygen ionic conductivity of $Tm_2(Tm_{2-x}Tm_x)O_{7-x/2}$ "stuffed" pyrochlores, Inorg. Chem. 60 (7) (2021) 4517–4530, doi:10.1021/acs.inorgchem.0c03363.
[27] R. Reisfeld, M. Zelner, A. Patra, Fluorescence study of zirconia films doped by Eu^{3+}, Tb^{3+} and Sm^{3+} and their comparison with silica films, J. Alloys Compd. 147 (2000) 300–301.

[28] S. Gutzov, M. Lerch, Optical properties of europium containing zirconium oxynitrides, Opt. Mater. 24 (2003) 547–554.
[29] A. Patra, Effect of crystal structure and concentration on luminescence in Er^{3+}:zrO_2 nanocrystals, Chem. Phys. Lett. 387 (2004) 35–39.
[30] M.M. Trexler, D. Zhang, L. Kelly, J. Sample, Crystal structure and optical properties of erbium- and neodymium-doped zirconia nanoparticles, J. Mater. Res. Soc. 25 (2010) 500–508, doi:10.1557/JMR.2010.0071.
[31] J.P. Zuniga, S.K. Gupta, M. Abdou, H.A. De Santiago, A.A. Puretzky, M.P. Thomas, B.S. Guiton, J. Lui, Y. Mao, Size, structure and luminescence of $Nd_2Zr_2O_7$ nanoparticles by molten salt synthesis, J. Mater. Sci. 54 (2019) 12411–12424.
[32] M. Martos, B. Julian-Lopez, E. Cordoncilli, P. Escribano, Structural and spectroscopic study of a novel erbium titanate pink pigment prepared by sol-gel methodology, J. Phys. Chem. B 112 (2008) 2319–2325.
[33] A.V. Shlyakhtina, S.N. Savvin, A.V. Levchenko, M.V. Boguslavskii, L.G. Shcherbakova, Heavily doped oxygen-ion conducting $Ln_{2+x}Ti_{2-x}O_{7-\delta}$ (Ln= Ho-Lu; x=0.44-0.81) pyrochlores: crystal structure, Microstruct. Electr. Conduct. Solid State Ion. 179 (2008) 985–991.
[34] A.V. Shlyakhtina, D.A. Belov, O.K. Karyagina, L.G. Shcherbakova, Ordering processes in Ln_2TiO_5 (Ln=Dy-Lu): the role of thermal history, J. Alloys Compd. 479 (2009) 6–10.
[35] A.V. Shlyakhtina, D.A. Belov, S.Y. Stefanovich, L.G. Shcherbakova, Nanostructuring phenomena in oxygen-conducting complex oxides of heavy REE, Russ. J. Electrochem. 47 (2011) 620–627.
[36] M.N. Aronov, Laboratory vibrating eccentric mill, Instruments Exp. Tech. 1 (1959) 153–154.
[37] M.N. Aronov, L.M. Morgulis. Certificate of authorship No. 113794.
[38] J.C.C. Abrantes, A. Levchenko, A.V. Shlyakhtina, L.G. Shcherbakova, A.L. Horovistiz, D.P. Fagg, J.R. Frade, Ionic and electronic conductivity of $Yb_{2+x}Ti_{2-x}O_{7-x/2}$ materials, Solid State Ion. 177 (2006) 1785–1788.
[39] J.P. Zuniga, S.K. Gupta, M. Pokhrel, Y. Mao, Exploring the optical properties of $La_2Hf_2O_7$:pr^{3+} nanoparticles under UV and X-ray excitation for potential lighting and scintillating applications, New J. Chem. 42 (12) (2018) 9381–9392.
[40] K.M. Turner, D.R. Rittman, R.A. Heymach, C.L. Tracy, M.L. Turner, A.F. Fuentes, W.L. Mao, R.C. Ewing, Pressure-induced structural modifications of rare-earth hafnate pyrochlore, J. Phys. 29 (25) (2017) 255401.
[41] M.A. Borik, T.V. Volkova, A.V. Kulebyakin, E.E. Lomonova, F.O. M.ilovich, V.A. Myzina, V.V. Osiko, P.A. Ryabochkina, N.Yu. Tabachkova, M.A. Uslamina, S.N. U.shakov, A.N. Chabushkin, J. Alloy. Compd. 621 (2015) 295–300.